ACS OMEGA

Open Access

http://pubs.acs.org/journal/acsodf

Article

Investigation on Compositional Structures of the Organic Matter and Biomarker Distributions in Shengli Lignite

Fang-Jing Liu,* Shan-Shan Gao, Zhi Yang, Bo Meng, Yun-Peng Zhao, Zai-Xing Huang, and Xian-Yong Wei

Cite This: *ACS Omega* 2024, 9, 3363−3372

Read Online

ACCESS | Metrics & More | Article Recommendations

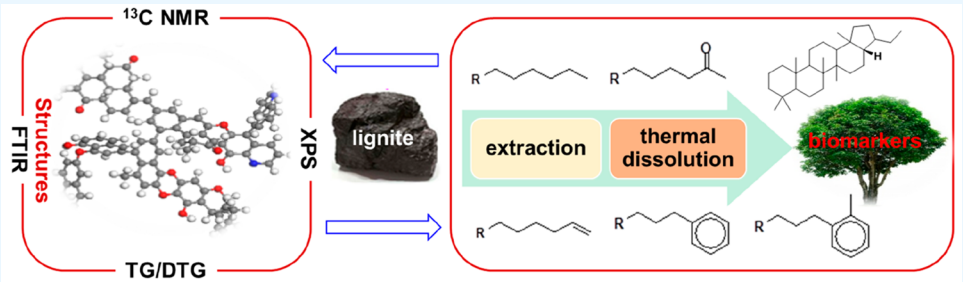

ABSTRACT: The structural characteristics of the organic matter and biomarker distributions in Shengli lignite (SL) were comprehensively studied by combining a variety of modern analytical techniques and solvent extraction/thermal dissolution. Characterization of SL with Fourier transform infrared spectroscopy, X-ray photoelectron spectroscopy, solid ^{13}C nuclear magnetic resonance spectroscopy and thermogravimetry showed that organic matter in SL is rich in oxygen functional groups, such as C−O, >C═O, and −COOH, and hydrogen bonds. The hydrogen bonds mainly include −OH···π, self-associated −OH, −OH···ether O, tightly bound cyclic −OH, −OH···N, −COOH dimers, and −SH···N. The highest content of organic nitrogen and sulfur on SL surface are pyrrole nitrogen and aromatic sulfur, respectively. The proportions of aromatic and aliphatic carbons in SL are about 58% and 39%, respectively. The aromatic carbon is mainly composed of protonated aromatic and aromatic bridged carbons; methylene carbon has the highest content among the aliphatic carbons, with chains of average length of 1.43 carbon atoms. The average number of aromatic structural units in the carbon skeleton of SL is about 3, and each aromatic structural unit contains an average of 1−2 substituent groups. Thermogravimetric analysis clarified the distribution of the main types of covalent bonds in SL and their possible cracking temperatures during pyrolysis. The extracts and soluble portion of thermal dissolution from SL were analyzed by a gas chromatograph/mass spectrometer, and a series of biomarkers were identified, mainly concentrated in petroleum ether extract and cyclohexane thermal soluble portion. These included long-chain *n*-alkanes, isoprenoid alkanes, long-chain *n*-alkenes, terpenoids, *n*-alkan-2-ones, long-chain *n*-alkylbenzene, and long-chain *n*-alkyltoluene. The comprehensive characterization of the organic matter and the distribution of related biomarkers provided an important scientific basis for understanding the molecular structural characteristics and geochemical information on SL.

1. INTRODUCTION

China is rich in lignite resources with proven reserves of more than 130 billion tons.[1] Because of its high moisture, high ash yield and high oxygen content, lignite is not suitable as a solid fuel for direct combustion. From the point view of the macromolecular structure of organic matter (OM), the aromatic rings in lignite (ca. 1−3 rings) are mainly connected by C−O and C−C bridged bonds, with C−O bridged bonds dominating and the aromatic ring bearing various alkyl side chain and oxygen-containing functional groups (OCFGs).[2,3] Although the structure of lignite OM plays an important role in its conversion, the in-depth understanding of its features at the molecular level is one of the core problems to be solved in coal chemistry. The solution of this issue would provide an important theoretical basis for the high-value-added utilization of these materials.

The studies on the structures of OM in lignite are oriented to evaluate the molecular structural features such as functional group and heteroatom distributions, bond types, carbon skeleton constitution (including aromatic ring and side chain distributions) and also its intermolecular and intramolecular

Received: September 2, 2023
Revised: December 10, 2023
Accepted: December 14, 2023
Published: January 9, 2024

Table 1. Proximate and Ultimate Analyses (wt %) of SL[a]

proximate analysis			ultimate analysis (daf)					
M_{ad}	A_d	V_{daf}	C	H	N	O_{diff}	$S_{t,d}$	H/C
20.40	19.00	37.85	69.26	5.50	0.86	23.23	1.15	0.95

[a]daf = dry and ash-free basis; M_{ad} = moisture (air-dried basis); A_d = ash (moisture-free basis); V_{daf} = volatile matter (dry and ash-free basis); O_{diff} = oxygen content, calculated by difference; $S_{t,d}$ = total sulfur (dry basis).

noncovalent interactions, such as hydrogen bonds and $\pi-\pi$ interactions.[1] For example, some reports have shown that noncovalent interactions in lignite, especially hydrogen bonding, have an important impact on lignite pyrolysis, liquefaction and thermal dissolution.[4−6] The OCFGs in lignite also have a significant effect on the yields of extracts and liquefaction products.[3] An in-depth understanding of the occurrence and structural characteristics of organic nitrogen in lignite is of great significance for studying the transfer mechanism of nitrogen and its effective removal during lignite conversion and utilization.[7−9] The authors previously found that oxidation under mild conditions is an effective way to obtain high-value-added benzenecarboxylic acids from lignite-derived residues. The yield and distribution of benzenecarboxylic acids depend on the structure and content of condensed aromatic rings in the residue.[10,11]

The methods used for studying coal structure include chemical, physical and physicochemical methods.[12] Advanced modern analytic techniques, such as elemental analysis, Fourier transform infrared (FTIR) spectroscopy,[13−15] nuclear magnetic resonance (NMR),[14,16,17] X-ray diffraction (XRD),[14,16,18] Raman spectroscopy,[14,18] and X-ray photoelectron spectroscopy (XPS)[16,19] are used for physical methods to directly study the elemental composition, functional groups, and carbon skeleton of coal, which can truly reflect the structural features of the OM in a nondestructive way.

Previous studies mostly used one or two modern analytical techniques to study the OM structure of lignite. However, this approach only provides partial structural information, so many interesting details can be easily overlooked. A combination of various modern analytic techniques could be a feasible approach for comprehensively studying the structure of. The low-rank lignite largely preserves the macromolecular structural features of the coal-forming plants, and it contains a series of biomarkers. Separation and identification of biomarkers in coal can not only provide important clues for the main input pathway of OM, coal-forming environment, and coal maturity but also provide important information on the structural features of OM in lignite. This latter plays an important role in the development and utilization of coal.[20] Solvent extraction combined with gas chromatography/mass spectrometry (GC/MS) technique is the most commonly used method for the isolation and identification of biomarkers from coal.[11,20,21]

In this study, advanced analytical techniques such as FTIR, XPS, solid ^{13}C NMR, and thermogravimetric analysis (TGA) were used for characterizing the OM in Shengli lignite (SL) in order to comprehensively obtain structural information on functional group distribution, surface element occurrence, carbon skeleton, and covalent bond types. GC/MS was adopted to analyze the distribution of biomarkers in soluble portions from SL in order to complement the structural information. The objective of this study is to provide insights into the structural features of the OM and the distributions of biomarkers in SL.

2. EXPERIMENTAL SECTION

2.1. Coal Samples and Reagents. SL was collected from Inner Mongolia Autonomous Region. It was pulverized and ground into powder with particle size <150 mesh followed by drying in vacuum at 80 °C for 24 h and storing in a desiccator before use. Its proximate and ultimate analyses are listed in Table 1. The organic solvents including petroleum ether (boiling range 60−90 °C), CS_2, acetone, methanol, and cyclohexane used in were purchased from Sinopharm Chemical Reagent Co., Ltd. and used after purification.

2.2. Direct Characterization of SL. The functional groups in SL were identified by infrared spectroscopy using a Nicolet Magna IR-560 FTIR spectrometer. The spectra were collected in the wavenumber range of 4000−400 cm^{-1} with 32 scans at a resolution of 4 cm^{-1}. The elements and their chemical forms on the SL surface were analyzed by a Thermo Fisher ESCALAB 250Xi XPS, which was equipped with a monochromatic Al Kα X-ray source with a power of 150 W and a beam spot size of 900 m. The fixed analyzer energy mode was used for the analysis, and the fixed transmission energy and step size were 20 and 0.05 eV, respectively. The fitting of narrow spectra of different elements were performed by using XPS PeakFit. The carbon skeleton structure features of OM in SL were analyzed by a Bruker Avance III spectrometer NMR equipped with a 4 mm cross-polarized magic-angle spinning (CP/MAS) dual-resonance probe, and the resonance frequency of ^{13}C was 100.63 MHz. The spectral width, recycle delay time, and contact time were 10 kHz, 0.5 s, and 1 ms, respectively. The NMR spectra were peak-fitted with PeakFit software. SL was analyzed with a Mettler Toledo TGA/DSC synchronous thermal analyzer. It was heated from room temperature to 110 °C at 10 °C/min. After holding at 110 °C for 10 min, the temperature was increased from 110 to 900 °C at 10 °C/min and maintained at 900 °C for 20 min.

2.3. Sequential Extraction and Thermal Dissolution of SL. According to the method reported in the literature,[8] 10 g of SL was sequentially extracted with 200 mL of petroleum ether, CS_2, methanol, acetone and isometric acetone/CS_2 at room temperature under ultrasonic conditions to obtain different extracts (denoted as E_1-E_5) and the extraction residue. Two grams of the extraction residue and 20 mL of cyclohexane were added into a 100 mL magnetic stirring autoclave reactor. The reactor was purged with N_2, quickly heated at 320 °C and magnetically stirred for 2 h.

After the reactor was cooled to room temperature, the solid−liquid mixture was recovered and filtered, followed by rinsing with cyclohexane. The solvent in the liquid phase was removed by a rotary evaporator to obtain the cyclohexane-soluble portion (CSP). The compositions of the small molecular compounds in E_1−E_5 and CSP were analyzed by GC/MS. The column in GC was heated from 50 to 300 °C with 6 °C/min and maintained at 300 °C for 15 min. The measured mass spectra were compared to the standard spectra in the NIST11a library for the compound assignment. The

https://doi.org/10.1021/acsomega.3c06615
ACS Omega 2024, 9, 3363−3372

molecular structure of the compound was determined according to the matching degree.

3. RESULTS AND DISCUSSION

3.1. Direct Characterization of the Organic Matter structure in SL.

3.1.1. Analysis with FTIR. As shown in Figure 1, the absorption peaks of functional groups, such as

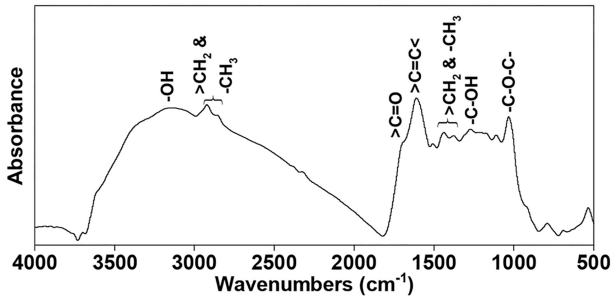

Figure 1. FTIR spectra of SL.

−OH (3300 cm^{-1}), $-CH_3$, and $>CH_2$ (2920 and 2850 cm^{-1}), >C═C< (1600 cm^{-1}), and C−O−C (1035 cm^{-1}), in SL have the highest intensity, which is consistent with the structural characteristics of common lignite. As shown in Figure 2, the

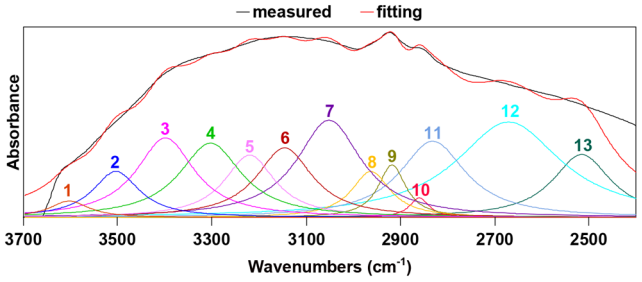

Figure 2. Curve-fitting of the 3600−2400 cm^{-1} region in the FTIR spectra of SL.

3700−2400 cm^{-1} region of FTIR spectrum is fitted into different peaks in order to study the type of hydrogen bonds in SL. The absorption peaks with different wavenumbers belong to different types of hydrogen bonds as reported previously.[22,23] As shown in Figure 2, the 3700−2400 cm^{-1} region of the FTIR spectrum is fitted into 13 peaks. Their corresponding assignments and relative contents are shown in Table 2. The results show that there are seven types of hydrogen bonds in SL as illustrated in Figure 3, and their absorption wavenumbers range between 3510 and 2500 cm^{-1}. As listed in Table 2, the highest content of −COOH dimer (peak 12) indicates that SL contains many carboxyl groups, which easily form strong hydrogen bonds. The −OH groups interacted with various functional groups or structures to form different types of hydrogen bonds (peaks 2−6), suggesting that SL is rich in −OH groups. The −SH···N type hydrogen bond (peak 13) could result from −SH of thiophenol or thiol and pyridine nitrogen. Hydrogen bonds play a vital role in forming and stabilizing the macromolecular network structure of lignite. Therefore, the hydrogen bonds in lignite are crucial to understanding its macromolecular structures and also affect its reactivity.[4−6]

Table 2. Assignments of the 3700−2400 cm^{-1} Region in the FTIR Spectra of SL

peak	wavenumber (cm^{-1})	assignment	relative area (%)
1	3601	free −OH	1.4
2	3500	−OH···π	4.5
3	3398	self-associated −OH	9.7
4	3300	−OH···ether O	9.7
5	3223	tightly bound cyclic −OH	6.6
6	3145	−OH···N (acid/base structures)	8.2
7	3050	aromatic CH stretching vibration	13.1
8	2964	CH_3 asymmetric stretching vibration	3.8
9	2918	CH_2 asymmetric stretching vibration	3.0
10	2855	CH_3 symmetric stretching vibration	0.8
11	2831	CH_3 symmetric stretching vibration	10.6
12	2670	−COOH dimers	21.0
13	2515	−SH···N	7.7

3.1.2. Analysis with XPS. XPS is widely used to determine the occurrence forms of elements on the surface of coal and its derivatives. The narrow spectra of C 1s, N 1s and S 2p of SL are fitted into different peaks, and the results are displayed in Figure 4 and Table 3. The C 1s spectrum can be divided into four peaks with binding energies of 284.8, 286.0, 287.2, and 289.1 eV, corresponding to different types of carbon. The relative content of aliphatic and aromatic carbon on the SL surface is 62.9%.

The relative content of OCFGs decreases in the order of C−OH or C−O > C═O > COOH. The C−OH or C−O with the highest content could be present in the forms of phenols, aliphatic alcohols, aromatic ethers, or aliphatic ethers. It can be seen from Table 1 that the content of nitrogen and sulfur in SL is low, but they will be released in the forms of NO_X and SO_X during the conversion of SL, causing serious pollution. Therefore, an in-depth understanding of the forms of nitrogen and sulfur in SL is of great scientific significance for the effective removal of nitrogen and sulfur in SL. As shown in Figure 4 and Table 3, nitrogen on the SL surface mainly includes pyridinic nitrogen, amino nitrogen, pyrrolic nitrogen, quaternary nitrogen, and pyridine oxide, with pyrrolic nitrogen having the highest content.

As shown in Figure 4 and Table 3, sulfur on the SL surface includes inorganic sulfur and organic sulfur, in which the inorganic sulfur is dominated by sulfate, with a relative content of 58.8%. Most of the organic sulfur present in SL is covalently bonded to the macromolecular network. The organic sulfur on the SL surface is primarily composed of aliphatic sulfur, aromatic sulfur, sulfoxide, and sulfone, and the content of the aromatic sulfur is the highest. Aliphatic sulfur may mainly exist in the forms of thiol, sulfide, and disulfide. Aromatic sulfur is mainly present in thiophene and its derivatives, such as benzothiophene and dibenzothiophene. The high content of sulfoxide and sulfone could be attributed to the oxidation of aliphatic sulfur and aromatic sulfur during transportation and storage.

3.1.3. Analysis with Solid ^{13}C NMR. Solid ^{13}C NMR is widely used to characterize the structural characteristics of the carbon skeleton in coal. The chemical shifts of different carbons and their assignments can refer to previous

https://doi.org/10.1021/acsomega.3c06615
ACS Omega 2024, 9, 3363−3372

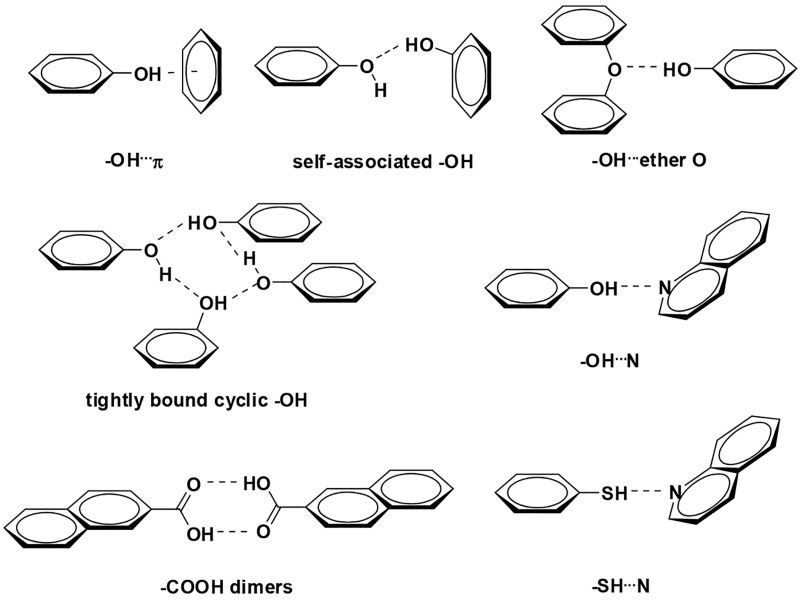

Figure 3. Different hydrogen bonds in SL.

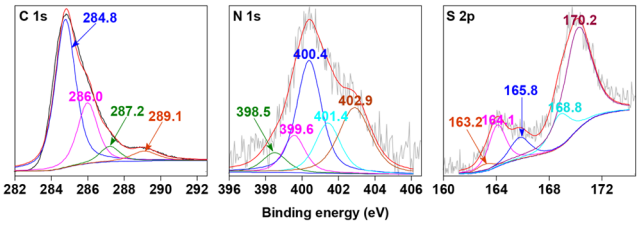

Figure 4. XPS C 1s, N 1s, and S 2p spectra and their fitting curves of SL.

Table 3. Distributions of Element Forms on the Surface of SL from XPS Analysis

element	binding energy (eV)	occurrence form	relative content (%)
C 1s	284.8	aliphatic and aromatic carbon	62.9
	286.0	C−OH or C−O	25.4
	287.2	C═O	6.4
	289.1	COOH	5.3
N 1s	398.5	pyridinic N	6.5
	399.6	amine	10.9
	400.4	pyrrolic N	37.4
	401.4	quaternary N	16.9
	402.9	pyridine oxide	28.3
S 2s	163.2	aliphatic sulfur	2.6
	164.1	aromatic sulfur	15.3
	165.8	sulfoxide	9.2
	168.8	sulfone	14.2
	170.2	sulfate	58.8

literature.[24−26] As shown in Figure 5, the ^{13}C NMR spectrum of SL can be divided into three sections: aliphatic carbon (δ = 0−90 ppm), aromatic carbon (δ = 90−170 ppm), and carbonyl carbon (δ = 170−220 ppm). The ^{13}C NMR spectrum of SL was further fitted into 16 peaks representing different types of carbon, and their chemical shifts, assignments, and molar percentages are listed in Table 4.

As illustrated in Figure 5 and Table 4, the carbon in SL is dominated by aliphatic and aromatic carbon with a low content of carbonyl carbon, and the content of aromatic carbon is significantly higher than that of aliphatic carbon. The $-\mathbf{C}H_2-$ (f_{al}^{3}) is the most abundant aliphatic carbon in SL, indicating that SL is rich in methylene moieties. SL also contains high content of methine and quaternary carbon. The CH_3 in SL is primarily present in the forms of $R\mathbf{C}H_3$ (f_{al}^{1}), $Ar\mathbf{C}H_3$ (f_{al}^{a}) and $\mathbf{C}H_3OCH_2-$ (f_{al}^{O1}), and their contents are relatively low.

As exhibited in Table 4, the aromatic carbon mainly includes protonated aromatic carbon (f_a^{H1}−f_a^{H3}), aromatic bridgehead carbon (f_a^{b}), alkylated aromatic carbon (f_a^{b}), and ArOH or ArOR carbon (f_a^{O}). Among them, f_a^{H1}−f_a^{H3} and f_a^{b} have the highest content, suggesting that the aromatic structure in SL is rich in protonated aromatic and aromatic bridgehead carbon. The alkylated aromatic carbon has remarkable higher content than ArOH or ArOR carbon. According to the results from ^{13}C NMR analysis, the OCFGs in SL in primarily present in CH_3OCH_2- (f_a^{O1}), $-CH_2OCH_2-$ (f_a^{O2}), RCH_2OH or >CHOH (f_a^{O3}), ArOH or ArOR (f_a^{O}), −COOH/−COOR (f_a^{C1}), and >C═O/−CHO (f_a^{C2}), and their content decreases in the order of $f_{al}^{O2} > f_a^{O} > f_a^{C1} > f_{al}^{O2} > f_a^{C2}$.

As displayed in Table 5, some key structural parameters of the carbon skeleton in SL were calculated according to the molar contents of the different carbons listed in Table 4. The aromatic condensation degree (f_a), aliphatic carbon ratio (f_{al}), and carbonyl carbon ratio (f_a^{C}) are approximately 58%, 39%, and 3%, respectively. It is speculated that each 100 carbon atoms in the carbon skeleton of SL contain approximately 58 aromatic carbons, 39 aliphatic carbons, and 3 carbonyl carbons, respectively. The bridged carbon ratio (x_b) is an important parameter indicating the size of aromatic unit in coal.[27,28] As listed in Table 4, the bridged carbon ratio of SL is 0.27, which is close to that of anthracene or phenanthrene (x_b = 0.29), indicating that the average number of the aromatic ring for each aromatic unit in SL is close to 3, which may be dominated by the anthracene or phenanthrene ring. The average length of the methylene chain of the carbon skeleton in SL is 1.43, implying that the methylene moiety in SL is dominated by

https://doi.org/10.1021/acsomega.3c06615
ACS Omega 2024, 9, 3363−3372

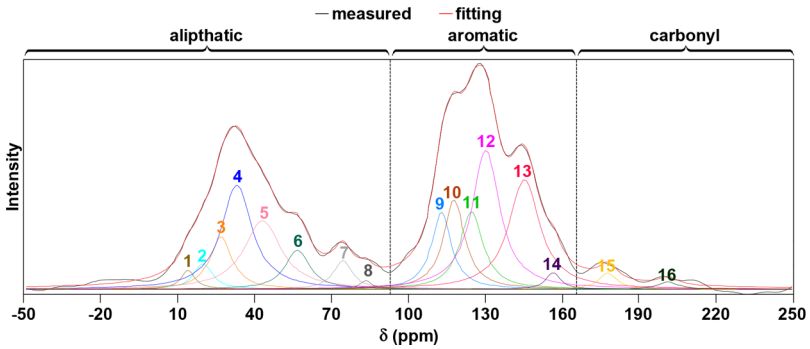

Figure 5. ^{13}C NMR spectrum of SL and its fitting curves.

Table 4. Chemical Shift and Molar Content (%) of Different Carbon Types in SL Analyzed by Solid-State ^{13}C NMR

peak	chemical shift (ppm)	assignment	symbol	molar content (%)
		aliphatic carbon		
1	14.0	RCH_3	f_{al}^1	2.2
2	19.9	$ArCH_3$	f_{al}^a	2.9
3	26.9	RCH_2CH_3	f_{al}^2	6.0
4	33.0	$-CH_2-$	f_{al}^3	11.8
5	43.0	tertiary CH and quaternary C	f_{al}^4	7.8
6	56.6	CH_3OCH_2-	f_{al}^{O1}	4.4
7	74.3	$-CH_2OCH_2-$	f_{al}^{O2}	3.3
8	83.3	RCH_2OH or >CHOH	f_{al}^{O3}	1.0
		aromatic carbon		
9	112.8	protonated aromatic	f_a^{H1}	8.8
10	117.7	protonated aromatic	f_a^{H2}	10.2
11	124.5	protonated aromatic	f_a^{H3}	8.8
12	130.0	bridgehead junction aromatic	f_a^b	15.8
13	145.1	side alkylated aromatic	f_a^a	12.4
14	156.3	ArOH or ArOR	f_a^O	1.9
		carbonyl carbon		
15	177.5	−COOH and −COOR	f_a^{C1}	1.8
16	201.0	>C=O and −CHO	f_a^{C2}	0.9

Table 5. Carbon Structural Parameters in SL Determined by Solid-State ^{13}C NMR

structural parameter	definition	value
aromaticity	$f_a = f_a^{H1} + f_a^{H2} + f_a^{H3} + f_a^b + f_a^a + f_a^O$	57.9%
aliphatic carbon ratio	$f_{al} = f_{al}^1 + f_{al}^a + f_{al}^2 + f_{al}^3 + f_{al}^4 + f_{al}^{O1} + f_{al}^{O2} + f_{al}^{O3}$	39.4%
carbonylation ratio	$f_a^C = f_a^{C1} + f_a^{C2}$	2.7%
bridgehead aromatic carbon ratio	$x_b = f_a^b/f_a$	0.27
avg carbon number of methylene	$C_n = (f_{al}^2 + f_{al}^3)/f_a^a$	1.43
substituted degree of aromatic ring	$\sigma = (f_a^a + f_a^O)/f_a$	0.25

short-chain methylene and alkyl side chains. The substituted degree (σ) of aromatic ring in the carbon skeleton of SL is about 0.25, indicating that the average number of substituent groups on each aromatic ring is 1−2.

3.1.4. Analysis with TGA. The weight loss below 350 °C in the TG curve of SL is mainly attributed to the removal of bound water, the release of volatile small molecules, and the decarboxylation. Pyrolysis of some covalent bonds in coal primarily occurs at 350−600 °C, releasing gases, volatile small molecules, and tar. Polycondensation of aromatic ring mainly occurs above 600 °C to release hydrogen and form semicoke.[29] As demonstrated in Figure 6, the weight loss mainly focuses between 350 and 700 °C, and the TG curve tends to be flat at temperature >700 °C. About 50% of SL reamins as resude at 900 °C, indicating that SL contains many stable structures that are not easily pyrolyzed, which is consistent with the results of solid ^{13}C NMR analysis that SL has high content of aromatic carbon. The cracking temperatures of different types of covalent bonds in lignite are different during pyrolysis. Therefore, the types of covalent bonds in lignite can be investigated by fitting the DTG curve. As shown in Figure 6, the DTG curve of SL can be divided into six peaks, and their peak temperature, corresponding covalent bond type and bond energy are presented in Table 6.[29]

As displayed in Figure 6 and Table 6, peak 1 with a peak temperature of 281 °C could be attributed to the release of bound water and decarboxylation in SL. Peak 2 with a peak temperature of 375 °C could be formed by the breaking of weak covalent bonds such as $C_{alk}-O$, $C_{alk}-N$, $C_{alk}-S$, and S−S, and their bond energy ranges between 150 and 230 kJ/mol. The peak temperature of peak 3 is 433 °C, which could be ascribed to the cleavage of $C_{alk}-C_{alk}$, $C_{alk}-H$, $C_{alk}-O$, and $C_{ar}-N$ with bond energies of 210−320 kJ/mol. SL is rich in these covalent bonds because they have the highest peak area. Peak 4 with a peak temperature of 543 °C could result from breakage of strong covalent bonds such as $C_{ar}-C_{alk}$, $C_{ar}-O$, and $C_{ar}-S$ with a bond energy of 300−430 kJ/mol. The weight loss above 700 °C during pyrolysis is mainly caused by the condensation of aromatic rings in coal to produce H_2 and the formation of semicoke.[29] The bond energy of $C_{ar}-H$ is generally higher than 400 kJ/mol, and the peak temperature of peak 6 is 771 °C.

3.2. Biomarker Distributions in SL. *3.2.1. Distribution of Group Components in E_1 and CSP.* Lignite largely retains the macromolecular structural characteristics of coal-forming plants and contains a series of biomarkers. The characterization of these biomarkers can provide important basis for the main input pathways and coal-forming environment of lignite and also provide important information on the structural characteristics of OM in lignite. The chemical compositions of small molecular compounds in E_1 and CSP was analyzed by GC/MS, and the distribution of the group components is presented in Figure 7. The relative contents of condensed aromatics (mainly 1-methylnaphthalene) and alkanes in E_1 are predominant. The types of group components in CSP are more abundant than E_1, mainly including alkanes, olefins, alkylbenzenes, condensed arenes, phenols, ketones, esters,

https://doi.org/10.1021/acsomega.3c06615
ACS Omega 2024, 9, 3363−3372

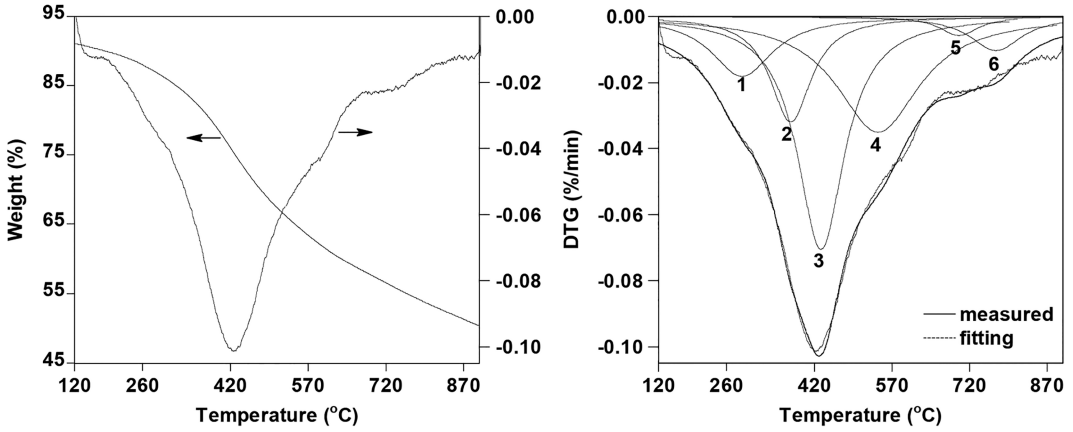

Figure 6. TG/DTG curve of SL and fitting curves of DTG curve.

Table 6. Assignment of Different Peaks from the DTG Profile of SL

peak	assignment	bond energy (kJ/mol)	peak temp
1	release of bound water and decarboxylation reaction	<150	281
2	cleavage of weak C_{alk}−O, C_{alk}−N, C_{alk}−S, and S−S bonds	150−230	375
3	cleavage of C_{alk}−C_{alk}, C_{alk}−H, C_{alk}−O, and C_{ar}−N bonds	210−320	433
4	cleavage of C_{ar}−C_{alk}, C_{ar}−O, and C_{ar}−S bonds	300−430	543
5	carbonate decomposition to produce CO_2		699
6	release of H_2 from aromatic ring condensation reaction	>400	771

nitrogen-containing compounds, and sulfur-containing compounds, among which the content of phenols is the highest.

Phenols were not found in E_1 but a large number of phenols were detected in CSP. It is speculated that phenols in lignite could be bonded with each other or other structures with strong noncovalent bonds, especially hydrogen bonds, or phenolic precursors are phenoxy groups bonded with macromolecular groups through weak C−O bonds. The FTIR analysis proves the presence of hydrogen bonds containing phenolic structures in SL (Figure 3). The TGA analysis shows that the C−O bond in SL is hardly broken at temperatures lower than 320 °C (Figure 6). Therefore, the phenols detected in CSP are mainly attributed to the dissociation of noncovalent bonds, especially hydrogen bonds, during the thermal dissolution. There is a series of biomarkers in the group components of E_1 and CSP.

3.2.2. Biomarkers in E_1. Alkanes are an important class of biomarkers in coal, indicating important sources of OM in coal. As shown in Figure 8a, *n*-alkanes in E_1 have a carbon number ranging from 9 to 35, and their relative contents show in a bimodal distribution. The *n*-alkanes with the highest content are *n*-tetradecane and *n*-heptacosane, respectively. The *n*-alkanes with a carbon number of C_{23}−C_{31} show an obvious odd carbon number predominance (OCNP), and the relative content of *n*-alkanes with a carbon number of C_{17}−C_{22} is lower than that of long-chain homologues. This result indicates that higher terrestrial plant waxes play an important role in the formation of OM in SL.[20,30] The OCNP could be related to a process where decarboxylation or dehydroxylation exceeded the reduction when the alkanoic acids and alkanols were converted to alkanes in a weakly reducing environment during the diagenesis stage of lignite. This processes could result in a higher content of *n*-alkanes with odd carbon number. The *n*-

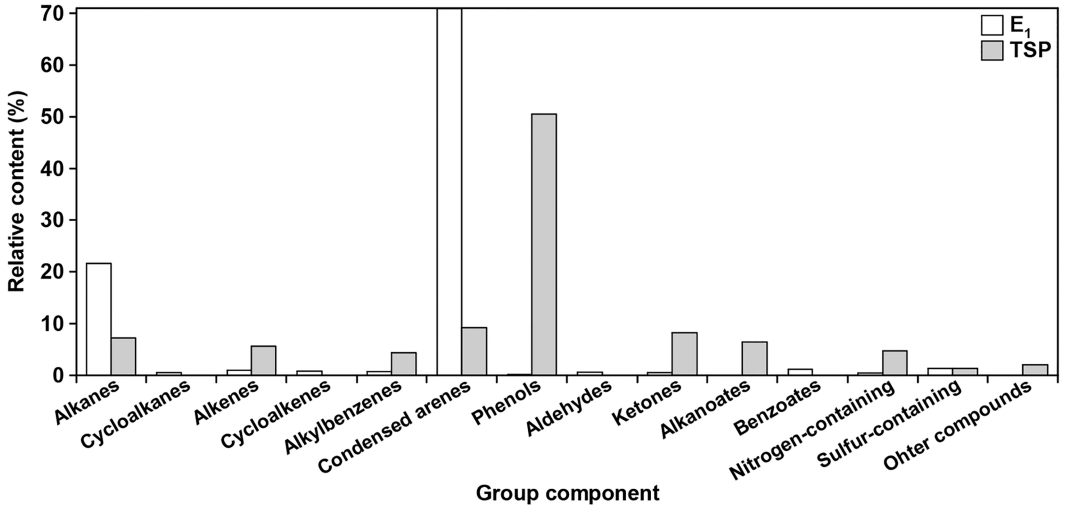

Figure 7. Group components in E_1 from ultrasonic extraction and CSP from thermal dissolution of SL by GC/MS analysis.

https://doi.org/10.1021/acsomega.3c06615
ACS Omega 2024, 9, 3363−3372

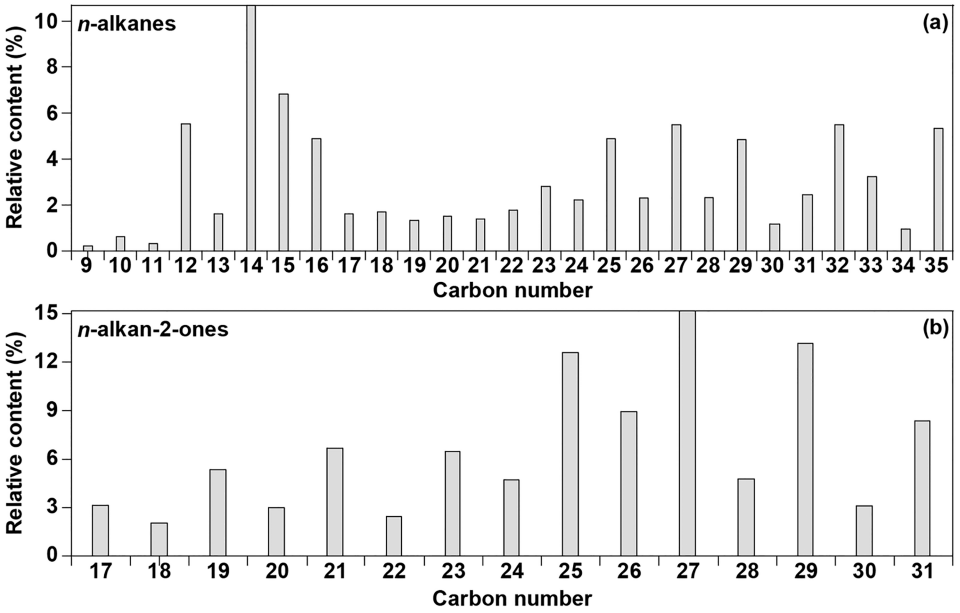

Figure 8. Distributions of (a) *n*-alkanes and (b) *n*-alkan-2-ones in E_1 from SL.

Table 7. Isoprenoid Alkanes and Terpenoids Identified in E_1 from SL

Compound	Molecular formula	Structural formula
Isohexadecane	$C_{16}H_{34}$	
Norpristane	$C_{17}H_{36}$	
Pristane	$C_{19}H_{40}$	
Phytane	$C_{20}H_{42}$	
18-Demethyl rosinane	$C_{19}H_{34}$	
17βH-Norhopane	$C_{29}H_{50}$	
Hop-22(29)-ene	$C_{30}H_{50}$	

alkanes with carbon numbers lower than 20 could result from bacteria and algae.

Isoprenoid alkanes, especially pristane and phytane, are important biomarkers indicating the diagenetic environment of coal sediments.[31] As shown in Table 7, isoprenoids such as isohexadecane, norpristane, pristane, and phytane were detected in E_1, with carbon number ranging from 15 to 20. These isoprenoids with carbon number less than 20 are called phytane series compounds, which could be mainly derived from chlorophyll of higher plants or pigment of bacteria/algae. Chlorophyll or bacteria/algae pigment decomposed to produce phytol in the presence of microorganisms, and phytol were further converted into isoprenoids during lignite diagenesis process. Terpenoids are also important biomarkers in coals and they have characteristic ion with m/z 191 in mass spectrum. Three terpenoids including 18-demethyl rosinane, 17βH-norhopane, and hop-22(29)-ene were detected in E_1. Terpenoids were dehydrogenated to form condensed aromatics in the diagenetic stage of lignite, which could be an important source of condensed aromatics in lignite.

As shown in Figure 8b, in addition to *n*-alkanes, a series of *n*-alkan-2-ones with carbon number distribution from 17 to 31 were detected in E_1. The contents of *n*-alkan-2-ones show a unimodal distribution and present an obvious OCNP with *n*-heptacos-2-one (C_{27}) having the highest content, which is similar to the distributions of *n*-alkanes with carbon numbers from 17 to 31. It is speculated that *n*-alkan-2-ones could be also converted from alkanoic acid or alkanols in higher plants. An isoprenoid methyl ketone, i.e., 6,10,14-trimethyl pentadecane-2-one, was also detected in E_1, which could be converted from phytol during coal diagenesis. A series of *n*-alkan-2-ones and 6,10,14-trimethylpentadecane-2-one were also detected in some immature coals,[20,32] suggesting that SL could also be a low mature coal. A series of *n*-alkan-2-ones with carbon number of C_{23}−C_{33} were also detected in higher plant wax and showed an obvious OCNP, suggesting that the *n*-alkan-2-ones in SL could be derived from higher plant wax.[20,33]

3.2.3. Biomarkers in CSP. A series of *n*-alkanes and isoprenoid alkanes (farnesane and norpristane) were also detected in CSP. The *n*-alkanes have carbon number ranging from 12 to 33, but there is no obvious OCNP. The distribution

https://doi.org/10.1021/acsomega.3c06615
ACS Omega 2024, 9, 3363−3372

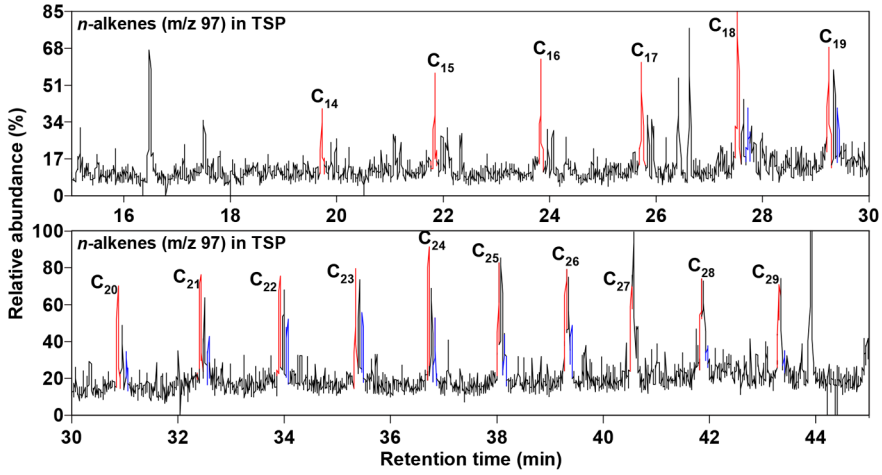

Figure 9. Selective ion chromatogram of *n*-alkenes in CSP (red and blue peaks represent *n*-alkan-1-enes and *n*-alkan-2-enes, respectively).

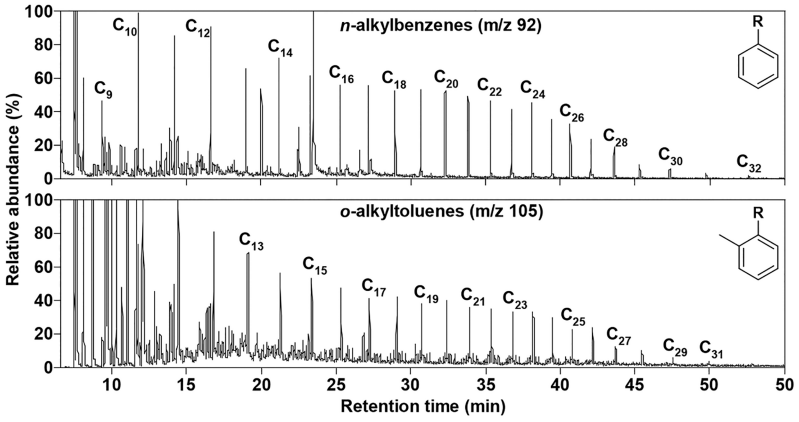

Figure 10. Selective ion chromatogram of *n*-alkylbenzenes and *n*-alkyltoluenes in CSP.

of *n*-alkenes was analyzed according to the selective ion chromatogram of m/z 97 (characteristic ion of *n*-alkenes) from the total ion chromatogram of CSP. As shown in Figure 9, two series of, i.e., *n*-alkan-1-enes and *n*-alkan-2-enes, were detected in CSP. The carbon number ranges of *n*-alkan-1-enes and *n*-alkan-2-enes are C_{14}−C_{29} and C_{18}−C_{29}, respectively. The relative content of *n*-alkan-1-ene is higher than *n*-alkan-2-ene for the isomer with the same carbon number. Although the formation pathway of *n*-alkenes during coal formation is not clear, they may be intermediates for the formation of *n*-alkane-2-ones from *n*-alkanes. E_1 and CSP are rich in compounds with methyl and methylene, such as *n*-alkanes, isoprenoid alkanes, and *n*-alkenes, which is consistent with solid ^{13}C NMR analysis that the aliphatic carbon in SL is dominated by methylene and methyl carbon.

Long-chain alkylbenzenes also provided key information about the organic geochemistry of coals. They have been confirmed to be present in coals[20,34] and coal-bed wax.[35] As displayed in Figure 10, a series of long-chain *n*-alkylbenzenes and *n*-alkyltoluenes were detected in CSP by extracting the selective ion chromatograms of alkylbenzenes (m/z 92) and alkyltoluenes (m/z 105). The base peaks of m/z 92 and 105 in the mass spectra of long-chain *n*-alkylbenzenes and *n*-alkyltoluenes are the ion fragments produced by the McLafferty rearrangement of γ-H on the alkyl side chain of the aromatic ring and β-cleavage. As illustrated in Figure 10, the carbon number distributions of long-chain *n*-alkylbenzenes and *n*-alkyltoluenes in CSP are C_9−C_{32} and C_{13}−C_{31}, and the corresponding carbon numbers of the alkyl side chains are C_3−C_{26} and C_6−C_{24}, respectively. It can be seen that the relative content of *n*-alkylbenzenes (except for the C_9 isomer) and *n*-alkyltoluenes generally decreases with an increase of the carbon number of alkyl side chains.

It was believed that the biogenic precursors of long-chain alkylbenzenes could be similar to alkanes, which could be mainly derived from *n*-alkanes and alkanols in terrigenous higher plants.[31] The previous study reported by the authors[20] suggested that *n*-alkanoic acids could undergo hydrogenation reduction, decarboxylation, hydrogen transfer, and cyclization to form long-chain *n*-alkylcyclohexane or *n*-alkylmethylcyclohexane, and they were further subjected to aromatization to form long-chain *n*-alkylbenzenes and *n*-alkyltoluenes. The pyrolysis of long-chain alkylbenzenes at high temperature to produce benzene, toluene, xylene, and long-chain alkanes could be an important source of light aromatics and long-chain alkanes in pyrolysis or gasification of coal tar.

4. CONCLUSIONS

The functional group distribution, surface element occurrence, carbon skeleton structure, and covalent bond type of SL were studied by FTIR, XPS, solid ^{13}C NMR, and TGA. The OM of SL is rich in OCFGs and contains seven different types of hydrogen bonds. The OCFGs mainly exist in the forms of C−OH or C−O, >C═O, and −COOH. The organic nitrogen on

https://doi.org/10.1021/acsomega.3c06615
ACS Omega 2024, 9, 3363−3372

the SL surface are primarily present in the forms of pyridinic nitrogen, amino nitrogen, pyrrolic nitrogen, quaternary nitrogen and pyridine oxide, and the content of pyrrolic nitrogen is the highest. The organic sulfur mainly includes aliphatic sulfur, aromatic sulfur, sulfoxide and sulfone, among which aromatic sulfur has the highest content. The OM in SL contains more aromatic carbon than aliphatic carbon. The aliphatic carbon is mainly composed of methylene, methine and quaternary carbon. The protonated aromatic carbon and aromatic bridged carbon have the highest content among the aromatic carbon. The average number of the aromatic ring for each aromatic unit in SL is about 3, which may be dominated by anthracene or phenanthrene ring. Each aromatic ring contains 1−2 substituents on average, and the methylene chain is mainly composed of short-chain methylene and short alkyl side chains. Different types of covalent bonds in SL and their cracking temperatures during pyrolysis were elucidated by TG/DTG analysis. The compositions of soluble organic small molecules in SL was revealed by solvent extraction and thermal dissolution. A series of biomarkers, such as long-chain *n*-alkanes, isoprenoid alkanes, long-chain *n*-alkenes, terpenoids, *n*-alkan-2-ones, long-chain *n*-alkylbenzenes, and long-chain *n*-alkyltoluenes, were identified. The input sources and formation pathways of these biomarkers were speculated, which provided important organic geochemical information for SL.

AUTHOR INFORMATION

Corresponding Author

Fang-Jing Liu − *Key Laboratory of Coal Processing and Efficient Utilization, Ministry of Education, China University of Mining and Technology, Xuzhou 221116 Jiangsu, China; Jiangsu Province Engineering Research Center of Fine Utilization of Carbon Resources, China University of Mining and Technology, Xuzhou 221116 Jiangsu, China; State Key Laboratory of Chemistry and Utilization of Carbon Based Energy Resources, Xinjiang University, Urumqi 830017 Xinjiang, China;* orcid.org/0000-0003-3101-2090; Email: fangjingliu@cumt.edu.cn

Authors

Shan-Shan Gao − *Key Laboratory of Coal Processing and Efficient Utilization, Ministry of Education, China University of Mining and Technology, Xuzhou 221116 Jiangsu, China*

Zhi Yang − *Key Laboratory of Coal Processing and Efficient Utilization, Ministry of Education, China University of Mining and Technology, Xuzhou 221116 Jiangsu, China*

Bo Meng − *Key Laboratory of Coal Processing and Efficient Utilization, Ministry of Education, China University of Mining and Technology, Xuzhou 221116 Jiangsu, China*

Yun-Peng Zhao − *Key Laboratory of Coal Processing and Efficient Utilization, Ministry of Education, China University of Mining and Technology, Xuzhou 221116 Jiangsu, China; Jiangsu Province Engineering Research Center of Fine Utilization of Carbon Resources, China University of Mining and Technology, Xuzhou 221116 Jiangsu, China;* orcid.org/0000-0001-8120-0060

Zai-Xing Huang − *Key Laboratory of Coal Processing and Efficient Utilization, Ministry of Education, China University of Mining and Technology, Xuzhou 221116 Jiangsu, China*

Xian-Yong Wei − *Key Laboratory of Coal Processing and Efficient Utilization, Ministry of Education, China University of Mining and Technology, Xuzhou 221116 Jiangsu, China; Jiangsu Province Engineering Research Center of Fine Utilization of Carbon Resources, China University of Mining and Technology, Xuzhou 221116 Jiangsu, China;* orcid.org/0000-0001-7106-4624

Complete contact information is available at: https://pubs.acs.org/10.1021/acsomega.3c06615

Notes

The authors declare no competing financial interest.

ACKNOWLEDGMENTS

This work was supported by the National Natural Science Foundation of China (Grant 22378415, 22178373) and State Key Laboratory of Chemistry and Utilization of Carbon Based Energy Resources (Grant KFKT2022002).

REFERENCES

(1) Liu, F.-J.; Wei, X.-Y.; Fan, M.; Zong, Z.-M. Separation and structural characterization of the value-added chemicals from mild degradation of lignites: A review. *Applied Energy* **2016**, *170*, 415−436.

(2) Mathews, J. P.; Chaffee, A. L. The molecular representations of coal−a review. *Fuel* **2012**, *96*, 1−14.

(3) Murata, S.; Hosokawa, M.; Kidena, K.; Nomura, M. Analysis of oxygen-functional groups in brown coals. *Fuel Process. Technol.* **2000**, *67* (3), 231−243.

(4) Miura, K. Mild conversion of coal for producing valuable chemicals. *Fuel Process. Technol.* **2000**, *62* (2), 119−135.

(5) Masaki, K.; Kashimura, N.; Takanohashi, T.; Sato, S.; Matsumura, A.; Saito, I. Effect of pretreatment with carbonic acid on "HyperCoal"(ash-free coal) production from low-rank coals. *Energy Fuels* **2005**, *19* (5), 2021−2025.

(6) Lei, Z.; Wu, L.; Zhang, Y.; Shui, H.; Wang, Z.; Ren, S. Effect of noncovalent bonds on the successive sequential extraction of Xianfeng lignite. *Fuel Process. Technol.* **2013**, *111*, 118−122.

(7) Kawashima, H.; Koyano, K.; Takanohashi, T. Changes in nitrogen functionality due to solvent extraction of coal during HyperCoal production. *Fuel Process. Technol.* **2013**, *106*, 275−280.

(8) Liu, F.-J.; Wei, X.-Y.; Gui, J.; Li, P.; Wang, Y.-G.; Li, W.-T.; Zong, Z.-M.; Fan, X.; Zhao, Y.-P. Characterization of organonitrogen species in Xianfeng lignite by sequential extraction and ruthenium ion-catalyzed oxidation. *Fuel Process. Technol.* **2014**, *126*, 199−206.

(9) Liu, F.-J.; Bie, L.-L.; Guo, J.-P.; Zong, Z.-M.; Wei, X.-Y. Occurrence forms and molecular structural characteristics of the organic nitrogen in lignite. *Journal of Fuel Chemistry and Technology* **2020**, *48* (7), 776−784.

(10) Liu, F.-J.; Zong, Z.-M.; Gui, J.; Zhu, X.-N.; Wei, X.-Y.; Bai, L. Selective production and characterization of aromatic carboxylic acids from Xianfeng lignite-derived residue by mild oxidation in aqueous H2O2 solution. *Fuel Process. Technol.* **2018**, *181*, 91−96.

(11) Liu, F.-J.; Zong, Z.-M.; Li, W.-T.; Zhu, X.-N.; Wei, X.-Y.; Tang, M.-C.; Huang, Z.-X. A three-step dissociation method for converting Xiaolongtan lignite into soluble organic compounds: Insights into chemicals, geochemical clues, and structural characteristics. *Fuel* **2019**, *242*, 883−892.

(12) Xie, K.-C. *Coal Structure and Its Reactivity*; Science Press: Beijing, 2002.

(13) Iglesias, M. J.; del Rio, J. C.; Laggoun-Défarge, F.; Cuesta, M. J.; Suárez-Ruiz, I. Control of the chemical structure of perhydrous coals; FTIR and Py-GC/MS investigation. *Journal of Analytical and Applied Pyrolysis* **2002**, *62* (1), 1−34.

(14) Baysal, M.; Yürüm, A.; Yıldız, B.; Yürüm, Y. Structure of some western Anatolia coals investigated by FTIR, Raman, 13C solid state NMR spectroscopy and X-ray diffraction. *International Journal of Coal Geology* **2016**, *163*, 166−176.

(15) Tian, B.; Qiao, Y.; Fan, J.; Li, P.; Zong, P.; Tian, Y. N-methyl-2-pyrrolidone/CS_2 extraction induced changes in surface and bulk structures of a lignite. *Journal of the Energy Institute* **2018**, *91* (5), 756−768.

(16) Lin, H.-L.; Li, K.-J.; Zhang, X.; Wang, H. Structure Characterization and Model Construction of Indonesian Brown Coal. *Energy Fuels* **2016**, *30* (5), 3809−3814.
(17) Hou, Y.; Yang, F.; Yang, C.; Feng, Z.; Feng, L.; Li, H.; Ren, S.; Wu, W. A study on the structure of anthracite based on benzene carboxylic acids. *Journal of the Energy Institute* **2021**, *98*, 153−160.
(18) Jiang, J.; Yang, W.; Cheng, Y.; Liu, Z.; Zhang, Q.; Zhao, K. Molecular structure characterization of middle-high rank coal via XRD, Raman and FTIR spectroscopy: Implications for coalification. *Fuel* **2019**, *239*, 559−572.
(19) Nowicki, P.; Pietrzak, R.; Wachowska, H. X-ray Photoelectron Spectroscopy Study of Nitrogen-Enriched Active Carbons Obtained by Ammoxidation and Chemical Activation of Brown and Bituminous Coals. *Energy Fuels* **2010**, *24* (2), 1197−1206.
(20) Liu, F.-J.; Wei, X.-Y.; Gui, J.; Wang, Y.-G.; Li, P.; Zong, Z.-M. Characterization of Biomarkers and Structural Features of Condensed Aromatics in Xianfeng Lignite. *Energy Fuels* **2013**, *27* (12), 7369−7378.
(21) Stojanović, K.; Životić, D. Comparative study of Serbian Miocene coals — Insights from biomarker composition. *International Journal of Coal Geology* **2013**, *107*, 3−23.
(22) Li, D.; Li, W.; Li, B. A new hydrogen bond in coal. *Energy Fuels* **2003**, *17* (3), 791−793.
(23) Chen, C.; Gao, J.; Yan, Y. Observation of the type of hydrogen bonds in coal by FTIR. *Energy Fuels* **1998**, *12* (3), 446−449.
(24) Yoshida, T.; Maekawa, Y. Characterization of coal structure by CP/MAS carbon-13 NMR spectrometry. *Fuel Process. Technol.* **1987**, *15*, 385−395.
(25) Song, C.; Hou, L.; Saini, A. K.; Hatcher, P. G.; Schobert, H. H. CPMAS 13C NMR and pyrolysis-GC-MS studies of structure and liquefaction reactions of Montana subbituminous coal. *Fuel Process. Technol.* **1993**, *34* (3), 249−276.
(26) Liu, F.-J.; Wei, X.-Y.; Zong, Z.-M.; Fan, M. Characterization of the Oxygenated Chemicals Produced from Supercritical Methanolysis of Modified Lignites. *Energy Fuels* **2016**, *30* (4), 2636−2646.
(27) Wang, S.; Tang, Y.; Schobert, H. H.; Guo, Y. n.; Su, Y. FTIR and 13C NMR Investigation of Coal Component of Late Permian Coals from Southern China. *Energy Fuels* **2011**, *25* (12), 5672−5677.
(28) Solum, M. S.; Pugmire, R. J.; Grant, D. M. Carbon-13 solid-state NMR of Argonne-premium coals. *Energy Fuels* **1989**, *3* (2), 187−193.
(29) Shi, L.; Liu, Q.; Guo, X.; Wu, W.; Liu, Z. Pyrolysis behavior and bonding information of coal—a TGA study. *Fuel Process. Technol.* **2013**, *108*, 125−132.
(30) Tissot, B.; Pelet, R.; Roucache, J.; Combaz, A. Alkanes as geochemical fossils indicators of geological environments. *Adv. Org. Geochem.* **1975**, 117−154.
(31) Dević, G. J.; Popović, Z. V. Biomarker and micropetrographic investigations of coal from the Krepoljin Brown Coal Basin Serbia. *International Journal of Coal Geology* **2013**, *105*, 48−59.
(32) Tuo, J.; Li, Q. Occurrence and distribution of long-chain acyclic ketones in immature coals. *Appl. Geochem.* **2005**, *20* (3), 553−568.
(33) Baker, E. Chemistry and morphology of plant epicuticular waxes. *Plant Cuticle*; Academic Press, 1982; pp 139−166.
(34) Radke, M.; Willsch, H. Generation of alkylbenzenes and benzo[b]thiophenes by artificial thermal maturation of sulfur-rich coal. *Fuel* **1993**, *72* (8), 1103−1108.
(35) Ji-Zhou, D.; Vorkink, W. P.; Lee, M. L. Origin of long-chain alkylcyclohexanes and alkylbenzenes in a coal-bed wax. *Geochim. Cosmochim. Acta* **1993**, *57* (4), 837−849.

https://doi.org/10.1021/acsomega.3c06615
ACS Omega 2024, 9, 3363−3372